



Climatic control on rapid exhumation along the Southern Himalayan Front

Rasmus C. Thiede^{a,*}, Bodo Bookhagen^{a,1}, J. Ramón Arrowsmith^{b,2},
Edward R. Sobel^{a,3}, Manfred R. Strecker^{a,4}

^a *Institut fuer Geowissenschaften, Universitaet Potsdam, Potsdam 14415, Germany*

^b *Department of Geological Sciences, Arizona State University, Tempe, AZ 85287, USA*

Received 29 July 2003; received in revised form 23 February 2004; accepted 19 March 2004

Abstract

Along the Southern Himalayan Front (SHF), areas with concentrated precipitation coincide with rapid exhumation, as indicated by young mineral cooling ages. Twenty new, young ($< 1-5$ Ma) apatite fission track (AFT) ages have been obtained from the Himalayan Crystalline Core along the Sutlej Valley, NW India. The AFT ages correlate with elevation, but show no spatial relationship to tectonic structures, such as the Main Central Thrust or the Southern Tibetan Fault System. Monsoonal precipitation in this region exerts a strong influence on erosional surface processes. Fluvial erosional unloading along the SHF is focused on high mountainous areas, where the orographic barrier forces out $>80\%$ of the annual precipitation. AFT cooling ages reveal a coincidence between rapid erosion and exhumation that is focused in a $\sim 50-70$ -km-wide sector of the Himalaya, rather than encompassing the entire orogen. Assuming simplified constant exhumation rates, the rocks of two age vs. elevation transects were exhumed at $\sim 1.4 \pm 0.2$ and $\sim 1.1 \pm 0.4$ mm/a with an average cooling rate of $\sim 40-50$ °C/Ma during Pliocene–Quaternary time. Following other recently published hypotheses regarding the relation between tectonics and climate in the Himalaya, we suggest that this concentrated loss of material was accommodated by motion along a back-stepping thrust to the south and a normal fault zone to the north as part of an extruding wedge. Climatically controlled erosional processes focus on this wedge and suggest that climatically controlled surface processes determine tectonic deformation in the internal part of the Himalaya.

© 2004 Elsevier B.V. All rights reserved.

Keywords: Himalaya; apatite fission track; geochronology; exhumation; erosion; precipitation

* Corresponding author. Tel.: +49-331-977-2908; fax: +49-331-977-5060.

E-mail addresses: thiede@geo.uni-potsdam.de (R.C. Thiede), bodo@geo.uni-potsdam.de (B. Bookhagen), ramon.arrowsmith@asu.edu (J.R. Arrowsmith), ed@geo.uni-potsdam.de (E.R. Sobel), strecker@geo.uni-potsdam.de (M.R. Strecker).

¹ Tel.: +49-331-977-2908; fax: +49-331-977-5060.

² Tel.: +1-480-965-3541; fax: +1-480-965-8102.

³ Tel.: +49-331-977-5403; fax: +49-331-977-5060.

⁴ Tel.: +49-331-977-5261; fax: +49-331-977-5060.

1. Introduction

High exhumation rates in orogens are driven by both tectonic convergence and climatically controlled erosion (e.g. [1–3]). Rock uplift generates topographic relief, thereby enhancing the possibilities for orographic precipitation, which in turn focuses erosion. Enhanced precipitation (1) controls effective hillslope erosional processes such as the triggering of land-

slides and debris flows, and (2) increases river discharge, which in addition to channel slope, is an important parameter of determining the stream-power law [2,4]. The fluvial incision rate, overall fluvial

erosion, and sediment evacuation are thus strengthened. In those sectors affected by concentrated erosion, deformation and the rock uplift will be focused in response to the regional compression [3]. The

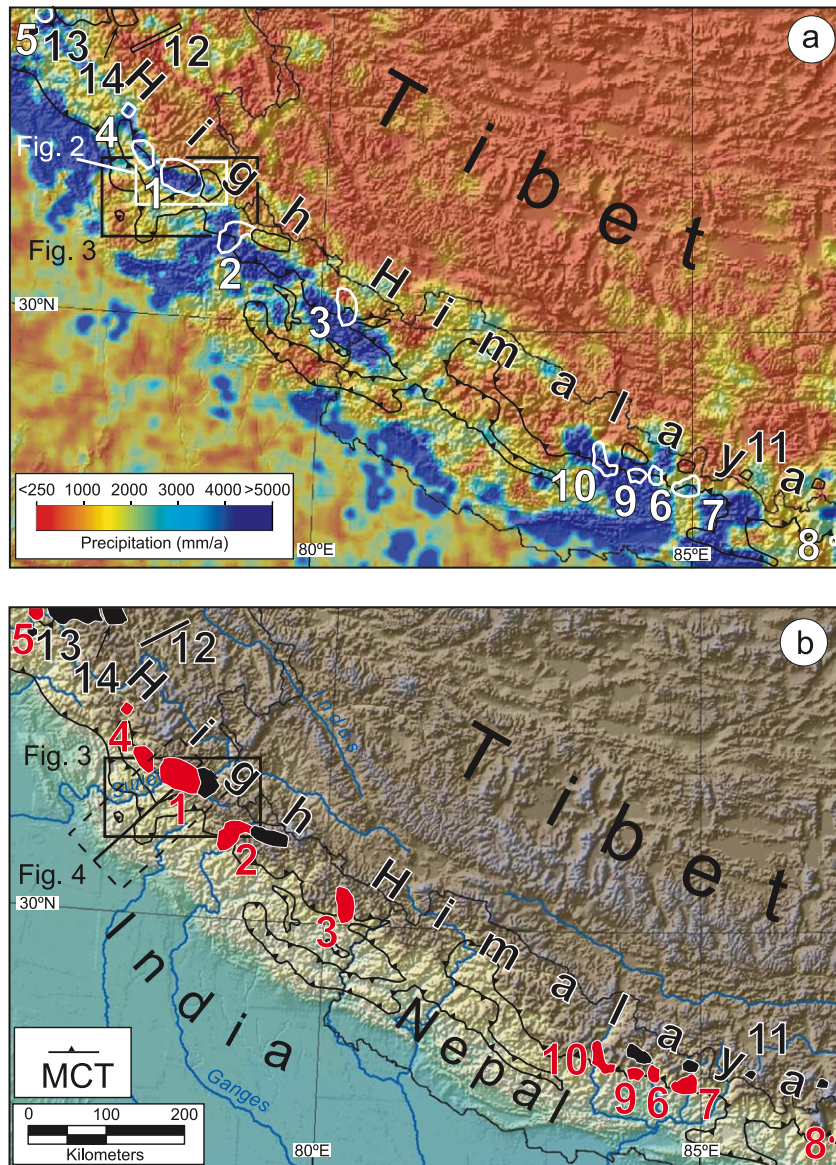


Fig. 1. Selected areas of young cooling ages (a) white polygons, (b) red polygons, with number referring to author (see Table 1) over (a) distribution of mean annual precipitation, and (b) topography of the central Himalaya (NW-India and Nepal). Young cooling ages from different geochronologic methods are localized along the southern termination of the High Himalaya, and overlap with regions of enhanced orographic precipitation during the Indian summer monsoon. Black and white boxes denote areas of detailed study along the Sutlej Valley in Figs. 2 and 3, black line in panel b is the cross-section in Fig. 4. Precipitation derived from calibrated SSM/I passive microwave data [13]. Shaded relief (1 km) and topography from GTOPO30 (USGS). The run of the MCT [27].

relationship between erosion and exhumation is primarily characterized by mass redistribution along river valleys running perpendicular to strike of a range, (e.g. [5,6]). Thereby two requirements must be accomplished in order to keep the positive feedback between erosion and exhumation operating over geologic time: (1) for high regional erosion, the river network has to provide sufficient runoff to cause high fluvial incision, erosion, and sediment flux to the foreland that exceeds local sediment flux generated by hillslope erosion. (2) Coeval mass removal must be balanced by tectonic influx of material to achieve steep channel gradients and relief, respectively. For instance, the concept of the critical taper model, (e.g. [7]), provides the framework to consider these processes. Thus, tectonically active regions with enhanced erosion are potentially subject to increased tectonic rates and may eventually influence spatial patterns of further rock uplift. However, the nature of this interaction between the distribution of precipitation, regional erosion rates, and patterns of rock uplift is still a matter of controversy, (e.g. [8–10]). For example, in central Nepal, Burbank et al. [8] find no significant spatial correlation between short-term precipitation and long-term erosion rates. These authors suggest that tectonically forced advection of crustal material is the most important factor affecting erosion across a region. Dadson et al. [10] propose for the Taiwan orogen that the patterns of erosion have changed over time in response to the migration of localized tectonic deformation. In contrast, Reiners et al. [9] show strongly varying long-term erosion rates across the Cascade Mountains (USA) closely tracking modern mean annual precipitation. Whereas Zeitler et al. [5] argues that within the syntaxial bends of the Himalaya the loci of deep and fast exhumation is caused by significant fluvial erosion. However, thermo-mechanical numerical models of Beaumont et al. [11] and Jamieson et al. [12] demonstrate how effective surface denudation may modify the internal deformation patterns of the Himalayan orogen.

Along the central part of the Southern Himalayan Front (SHF), monsoonal precipitation controlled by topography exerts a strong control on erosional processes, as these regions coincide with sectors of massive landsliding, debris-flow activity, and effective mass removal by streams [13] (Fig. 1a). These sectors of concentrated precipitation also coincide

Table 1

Selected areas of young cooling ages from the SHF (no. 1–10, Fig. 1) and Miocene AFT ages from the arid part of the High Himalaya (no. 11–14, Fig. 1)

No.	Region	Dating method	Age (Ma)	Authors
1	Sutlej Valley	FT-apatite	<1–4	Jain et al. [18]; Vanney et al. [6]; this paper
		FT-zircon	2–15	Jain et al. [18]; Vanney et al. [6]
2	Bhagirathi Valley	FT-apatite	1–4	Sorkhabi et al. [55]; Searle et al. [56]
		K/Ar-muscovite	5–22	Metcalfe [15]
		Th–Pb-monazite	5–22	Catlos et al. [20]
3	Gori Ganga Valley	FT-apatite	<1–2	Bojar et al. [79]
		Ar/Ar-white mica	12–14	Bojar et al. [79]
4	Bandal and Rotang	FT-apatite	2–4	Lal et al. [54]
5	Kishtwar Window	FT-apatite	1–4	Kumar et al. [58]
6	Marsyandi Valley	Ar/Ar-biotite	4–12	Edwards [94]
		FT-apatite	<1–4	Burbank et al. [8]
		Ar/Ar-white mica	2–10	Catlos et al. [19]
		Th–Pb-monazite	3–22	Catlos et al. [19]
7	Buhri Gandaki Valley	Ar/Ar-white mica	3–10	Copeland et al. [14]
		Ar/Ar-biotite	3–14	Copeland et al. [14]
		Th–Pb-monazite	4–8	Harrison et al. [16]
8	Dudh Kosi Valley	Th–Pb-monazite	11–16	Catlos et al. [20]
9	Ampipal	FT-apatite	1–2	Gautam and Koshimizu [95]
10	Modhi Valley/Kali Gandaki	FT-zircon	1–2.5	Arita [96]
11	Shisha Pangma	FT-apatite	12–15	Searle et al. [80]
12	Ladakh	FT-apatite	8–40	Schlup et al. [81]
13	Bhot Nala	FT-apatite	2–8	Kumar et al. [58]
14	Padam-Zanskar	FT-apatite	6–12	Kumar et al. [58]

FT—fission track, Ar/Ar— $^{40}\text{Ar}/^{39}\text{Ar}$, K/Ar— $^{40}\text{K}/^{40}\text{Ar}$, Th–Pb—in situ Th–Pb ion microprobe dating.

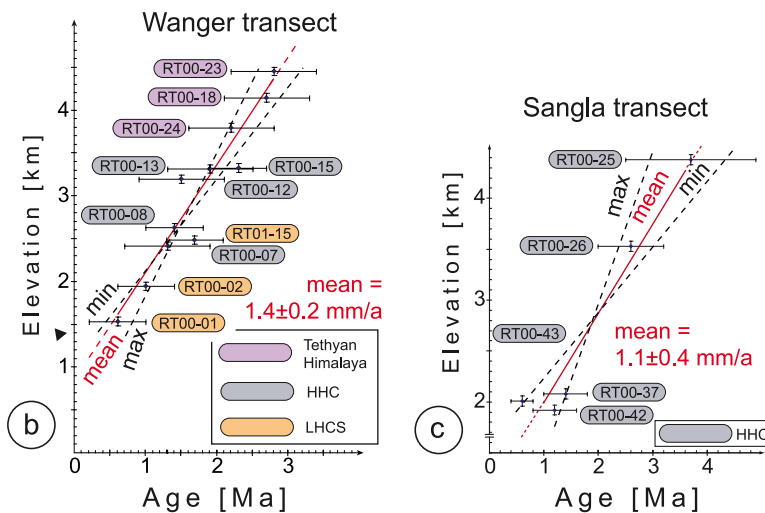
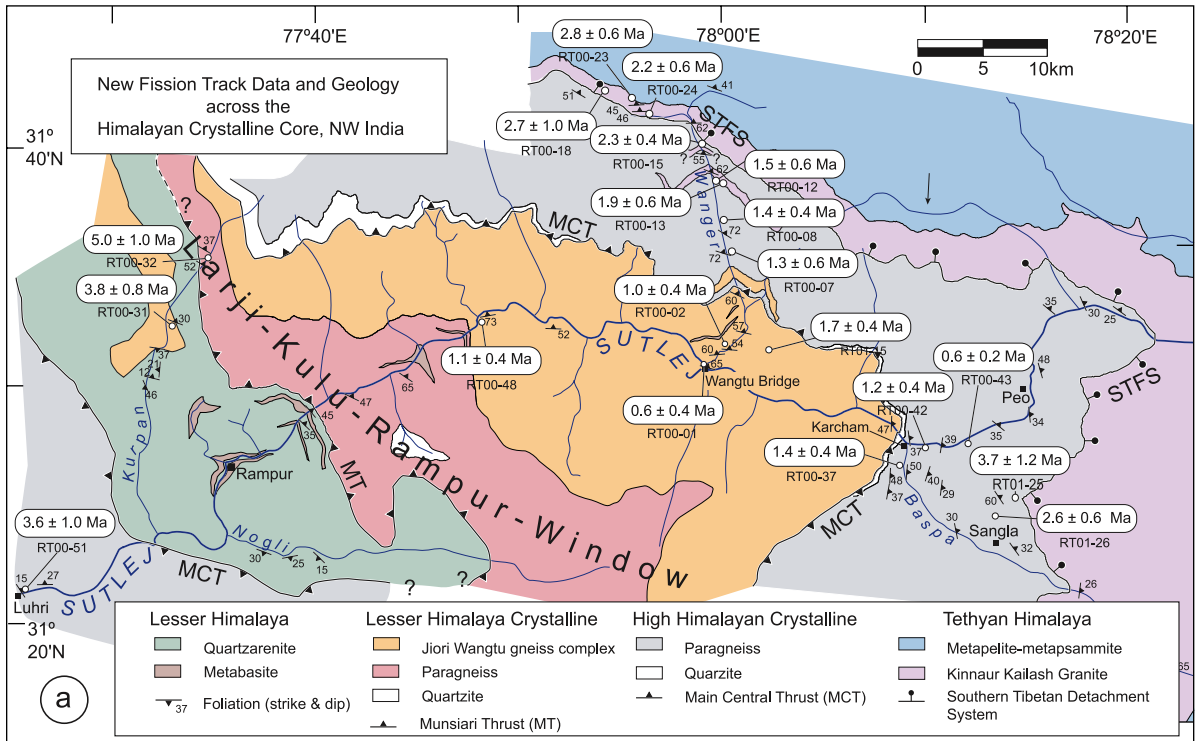


Fig. 2. (a) New apatite fission track ages (this study, errors are $\pm 2\sigma$) across the Himalayan Crystalline Core of Sutlej region. AFT cooling ages document young exhumation in the upper Sutlej Valley, where in a tectonic window rocks related to the Lesser Himalaya are exposed, surrounded by Higher Himalayan Crystalline rocks. Base geology modified from Vanney and Grasemann [30,37] with our observations. (b) Age vs. elevation transect along the Wanger Valley across the MCT and STFS. (c) Age vs. elevation transect from the hanging wall of the MCT in the Sangla area. Note that the transects shows no sensitivity to tectonic structures such as MCT and STFS, but rather the age correlates with elevation (see text for exhumation rate calculation/estimate).

Table 2

Apatite fission track data from the Sutlej Region, see Fig. 2 for location

Sample number	Altitude (m)	Latitude (DM)	Longitude (DM)	Rock type	Formation	#Xls	Spontaneous		Induced		Dosimeter		χ^2 <i>P</i> (%)	Pooled age (Ma)	$\pm 2\sigma$	Uran. (ppm)
							Rho-S	Ns	Rho-I	Ni	Rho-D	Nd				
RT00–1	1540	N 31°32.283'	E 078°0.171'	orthogneiss	LHCS	55	0.016	7	6.925	3093	13.184	8028	82	0.6	0.4	6.6
RT00–2	1950	N 31°33.102'	E 078°1.191'	orthogneiss	LHCS	45	0.076	37	19.673	9605	13.256	8028	97	1.0	0.4	19.2
RT00–7	2420	N 31°37.950'	E 078°2.553'	orthogneiss	LHCS	54	0.034	16	6.808	3208	13.328	8028	91	1.3	0.6	6.8
RT00–8	2640	N 31°38.863'	E 078°0.938'	gneiss	HHC	42	0.223	104	40.857	19,072	13.400	8028	100	1.4	0.4	36.4
RT00–12	3200	N 31°41.806'	E 078°0.081'	orthogneiss	HHC	30	0.075	23	12.858	3925	13.472	8028	96	1.5	0.6	11.8
RT00–13	3320	N 31°41.463'	E 078°0.485'	orthogneiss	HHC	33	0.191	74	26.690	10,320	13.544	8028	100	1.9	0.6	24.4
RT00–15	3330	N 31°42.656'	E 077°59.466'	orthogneiss	HHC	30	0.585	151	67.607	17,460	13.616	8028	100	2.3	0.4	60.2
RT00–18	4150	N 31°43.548'	E 077°54.748'	orthogneiss	KKG-TH	31	0.177	39	17.352	3813	13.688	8028	91	2.7	1.0	15.4
RT00–23	4460	N 31°43.429'	E 077°56.267'	orthogneiss	KKG-TH	35	0.609	239	57.571	22,580	13.760	8028	98	2.8	0.6	51.7
RT00–24	3800	N 31°42.957'	E 077°56.779'	orthogneiss	HHC	37	0.226	90	27.209	10,844	13.832	8028	98	2.2	0.6	23.6
RT00–31	2250	N 31°32.486'	E 077°34.606'	gneiss	LHCS	29	0.603	159	43.117	11,375	13.904	8028	65	3.8	0.8	36.3
RT00–32	2200	N 31°35.099'	E 077°35.344'	gneiss	LHCS	24	0.735	157	39.853	8509	13.976	8028	96	5.0	1.0	33.9
RT00–37	2080	N 31°48.767'	E 078°10.622'	gneiss/ mylonite	HHC	45	0.228	104	44.440	20,242	14.048	8028	81	1.4	0.4	40.0
RT00–42	1920	N 31°29.539'	E 078°12.023'	paragneiss/ mylonite	HHC	56	0.096	64	22.782	15,168	14.120	8028	93	1.2	0.4	20.0
RT00–43	2010	N 31°29.799'	E 078°13.211'	paragneiss/ mylonite	HHC	46	0.048	29	21.246	12,811	14.192	8028	91	0.6	0.2	17.1
RT00–48	1625	N 31°34.019'	E 077°49.865'	orthogneiss	LHCS	42	0.106	35	21.287	7050	11.037	6644	100	1.1	0.4	24.8
RT00–51	900	N 31°20.752'	E 077°26.482'	orthogneiss/ mylonite	HHC	29	0.247	55	15.080	3352	11.095	6644	100	3.6	1.0	16.4
RT01–15	2470	N 31°33.805'	E 078°04.210'	orthogneiss	LHCS	19	0.283	67	37.480	8861	11.449	4754	66	1.7	0.4	40.5
RT01–25	4380	N 31°27.013'	E 078°15.012'	gneiss/ mylonite	HHC	44	0.099	48	5.990	2897	11.478	4754	100	3.7	1.2	7.1
RT01–26	3530	N 31°27.247'	E 078°15.775'	gneiss/ mylonite	HHC	24	0.357	138	30.834	11,904	11.508	4754	92	2.6	0.6	31.7

Abbreviations are: LHCS, Lesser Himalaya Crystalline Sequence; HHCS, High Himalayan Crystalline Sequence; KKG-TH, Kinnauer Kailash Granite-Tethyan Himalaya; #Xls, number of individual grains dated; Rho-D, induced track density in external detector adjacent to dosimetry glass ($\times 10^6$ tracks/cm²); Nd, number of tracks counted in determining Rho-D; Rho-S, spontaneous track density ($\times 10^6$ tracks/cm²); Ns, number of spontaneous tracks counted; Rho-I, induced track density in external detector (muscovite) ($\times 10^6$ tracks/cm²); Ni, number of induced tracks counted; $\chi^2 P$ (%), chi-square probability [87,88]; Age is the sample pooled fission track age [90]; calculated using zeta calibration method [89]. Trackkey was used for calculating the counting results [92].

The following is a summary of key laboratory procedures. Samples were all analyzed by R. Thiede (zeta factor of 391 ± 27). Apatites were etched for 20 s in 5.5 N nitric acid at a temperature of 21 ± 0.1 °C. CN5 dosimetry glass was used as a neutron flux monitor. Samples were irradiated at Oregon State University TIRGA reactor. External detectors were etched in 40% HF. Tracks were counted with a Leica microscope with $100 \times$ air objective, $1.25 \times$ tube factor, $10 \times$ eyepieces, using transmitted light with supplementary reflected light as needed; external detector prints were located with Kinetek computer-automated scanning stage [91].

The AFT analysis employs the external detector method following the zeta calibration approach of Hurford and Green [90]. Analytical precisions of 0.2 to 1.0 Ma ($\pm 2\sigma$) could be obtained from these young AFT ages due to the high U-content and the large number of grains counted per sample. Only grains with *c* axes parallel to slide plane were dated and zero-track grains were considered.

with rapid exhumation, indicated by young mineral cooling ages of different isotopic systems, (e.g. [6,14–20]) (see Fig. 1 and Table 1). Assuming that the climatically driven erosional processes have been sustained over geologic time, and have not shifted spatially, large quantities of material should have been removed from these regions. This resulted in a situation where mass removal is compensated by renewed rock uplift and deformation. The similar tectonic history, structural setting, rock types, and pronounced precipitation gradients thus make the Himalayan arc a prime location to assess the complex linkages between tectonics, climate, and exhumation patterns.

In this study, we present 20 new, young (<1–5 Ma) apatite fission track (AFT) ages (Fig. 2 and Table 2) that were obtained across the crystalline core along the Sutlej Valley, NW India. The samples were collected in elevation transects across

major tectonic boundaries, such as the Main Central Thrust (MCT) and Southern Tibetan Fault System (STFS). This region coincides with a sector of the orogen where precipitation is concentrated and surface processes are vigorous [13]. Previous studies along the Sutlej Valley by Jain et al. [18] and Vannay et al. [6] reveal a zone of young cooling ages in the footwall of the MCT based on various geochronologic systems (AFT, <1–2 Ma, Fig. 3; zircon fission track—ZFT, 2–3 Ma; $^{40}\text{Ar}/^{39}\text{Ar}$, 4–6 Ma). We use our new AFT ages combined with published data to (1) determine the spatial distribution of exhumation in the Sutlej region, (2) map out the regional exhumation pattern in NW India to identify zones with high exhumation rates, and (3) to evaluate the correlation between high exhumation and areas of concentrated precipitation and enhanced erosion.

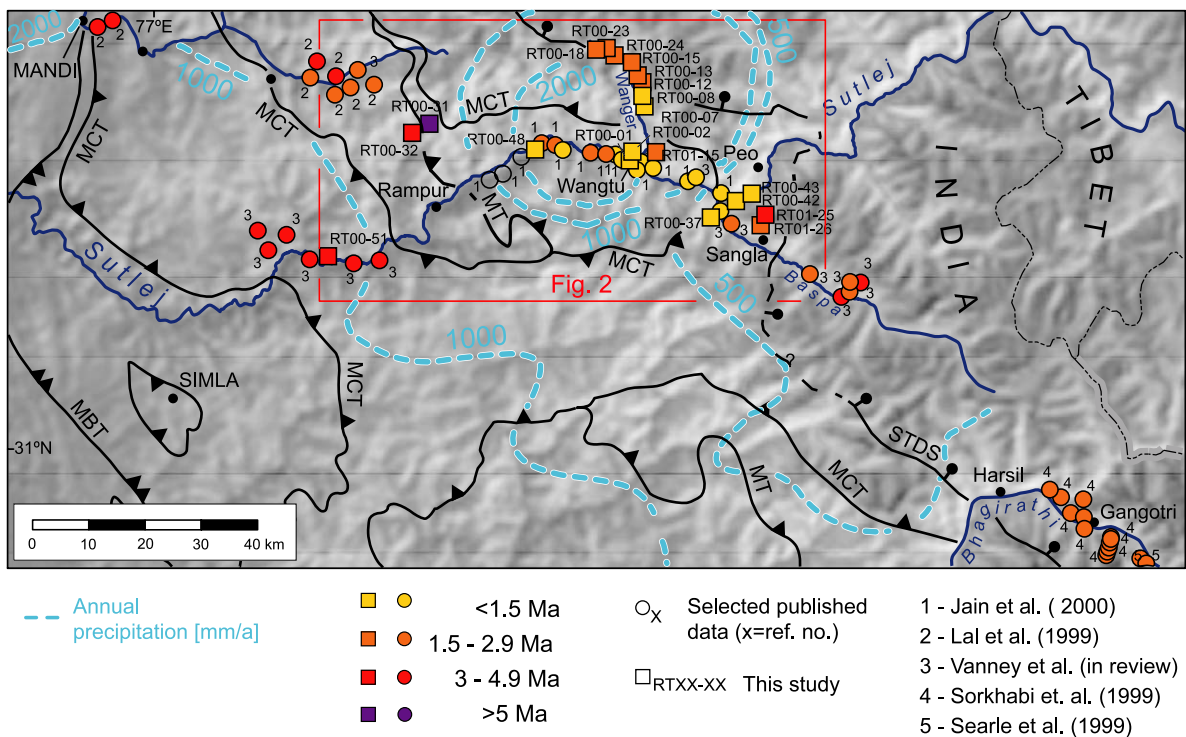


Fig. 3. Compiled AFT cooling ages across the crystalline core of the Himalaya (NW India) showing pronounced young ages in a ~50–70-km-wide sector of the deformation belt. Note the strong focusing of high regional precipitation and young cooling ages across the High Himalaya. Red box denotes area of detailed study along the Sutlej Valley (Fig. 2). Precipitation derived from calibrated SSM/I passive microwave data see Bookhagen et al. [13], and topography based on GTOPO30 (USGS). Tectonic structures modified after Vannay and Grasemann [37].

2. The Himalaya

The Himalayan orogen is the type location of an active continent–continent collision zone. It forms the

southern part of the collision zone between India and Asia and results from continued convergence and crustal thickening over the last ~ 50 Ma ([21,22] and references therein). Geodetic measurements, seis-

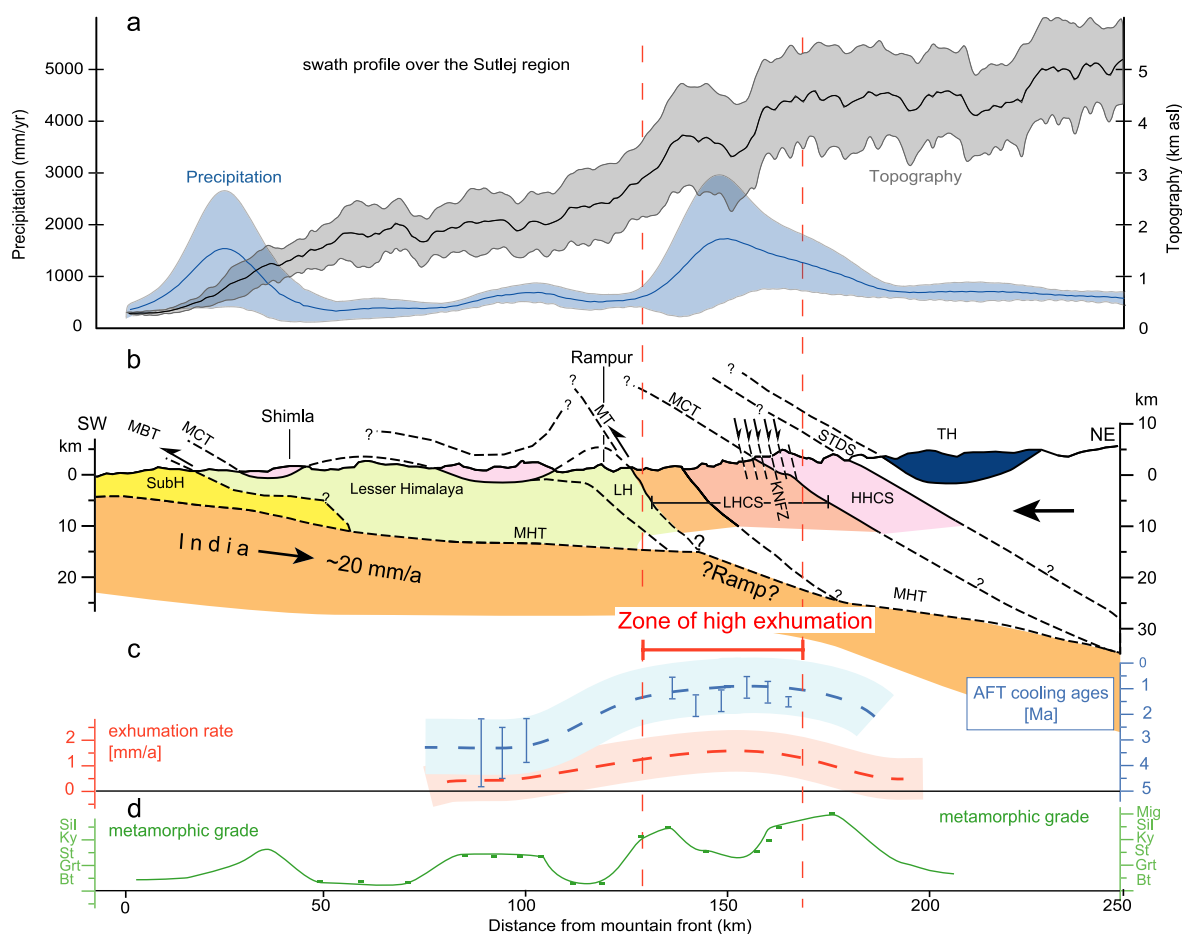


Fig. 4. (a) Compiled data illustrate the coupling between surface processes and tectonism in the Sutlej Region. Topographic (grey) and precipitation–distribution (blue) swath profiles for the Sutlej area are oriented perpendicular to the SHF. Swath profiles centered along the river are 250 km long and 100 km wide; thick, colored lines indicate mean values, shaded areas denote $\pm 2\sigma$. Topography based on (USGS), mean annual precipitation is derived from SSM/I passive microwave satellite data (see Bookhagen et al. [13] for more details). Note that the distribution of orographic precipitation is focused between elevations of ~ 2000 and ~ 3500 m in a ~ 50 – 70 -km-wide zone. (b) The simplified geologic cross-section parallel to the swath profiles shows that rocks of the LHCS in the footwall of the MCT are exhumed in this sector (geology modified from Vannay et al. [37] and this study). (c) Parallel to the geologic cross-section are AFT cooling ages along the Sutlej River shown (blue) and estimated exhumation rates (red); dashed lines indicate mean values, shaded areas denote $\pm 2\sigma$. In panel (d) the metamorphic grade of the rocks units along the profile is plotted (modified after Vannay et al. [93]). Based on AFT cooling ages (c), the coincidence between rapid erosion and exhumation is focused in a ~ 50 – 70 -km-wide sector of the Himalayan deformation belt, rather than encompassing the entire orogen. We assume that the enhanced and focused orographic precipitation (a) has localized rapid erosion and exhumation over geologic time. To accommodate this concentrated loss of material, deeper high-grade metamorphic rocks are exhumed (d) by motion along a back-stepping thrust to the south (MT) and normal fault zone (KNFZ) to the north (b) that is localized by climatically controlled erosional processes. TH, Tethyan Himalaya; HHCS, High Himalayan Crystalline Sequence; LHCS, Lesser Himalayan Crystalline Sequence; LH, Lesser Himalaya; SubH, Sub Himalaya; STFS, Southern Tibetan Fault System; MCT, Main Central Thrust; KNFZ, Karcham Normal Fault Zone; MT, Munsiari Thrust; MBT, Main Boundary Thrust; MHT, Main Himalayan Thrust.

micity, and both steep topography ($\sim 33^\circ$) and river-profile gradients (order of magnitude change) document ongoing convergence, deformation and uplift [23–26]. The kinematic evolution of the orogen is mainly controlled by the progressive action of a series of first-order crustal fault systems (STFS, MCT, Main Boundary Thrust—MBT, Main Frontal Thrust—MFT). These bound orogen-parallel tectonostratigraphic domains (Tethyan Himalaya (TH), High Himalayan Crystalline Sequence (HHCS), Lesser Himalaya (LH), and Sub-Himalaya), which have been detached along the Main Himalayan Thrust (MHT) from the underthrusting Indian plate and became incorporated into the orogen [22,27–29].

Along the Sutlej Valley in the northwestern sector of the orogen, the crystalline core of the Himalaya is exposed in two distinct gneiss units, characterized by different cooling histories ([6,30]; see Fig. 2). To the north, the HHCS, a ~ 10 km thick, NE-dipping sequence of highly deformed amphibolite to migmatic ortho- and paragneisses is bounded by the Early–Mid Miocene MCT at the base [31,32], and by the probably contemporaneously active extensional STFS at the top, e.g. [33–35]. The HHCS is interpreted to have been deformed as a southward extruding crystalline wedge [36,37]. Beneath the MCT, rocks related to the Lesser Himalayan Crystalline Sequence (LHCS) or of the MCT zone [38] are exposed in the tectonic Larji–Kulu–Rampur Window (LKRW) [39] along the Sutlej. These rocks are predominantly composed of amphibolite facies augen- and paragneisses [30,40]. Based on structural and geochronologic analysis [6], these rock units are interpreted to be a younger southward extruding wedge bounded at the base by the Munsiri Thrust (MT, active from Mid Miocene until recent) and at the top by a passive normal fault (Karcham Normal Fault Zone (KNFZ), e.g. [41]). Numerous hot springs, and carbonate and sulfur-rich precipitates along cataclastic zones characterize the LHCS and the lower part of the HHCS. Toward the foreland, the MCT becomes a shallow-dipping thrust, separating the HHCS from the low-to medium-grade metamorphic sediments of the Lesser Himalaya [30].

The central part of the Himalaya is characterized by a topographic discontinuity with a ~ 100 – 150 km wide, moderately elevated segment (< 3000 m asl) to the south-west, and the High Himalaya, a highly elevated segment with peaks of > 6000 m asl, high

relief, and steep slopes to the north-east (Fig. 1b). This abrupt change in topography beneath the front of the High Himalaya might be the result of motion along a crustal ramp in the MHT and/or fault bend fold structures in the LH, e.g. ([24,27,42,43]; see Fig. 4). Alternatively, it has been interpreted to be the result of recently active thrust faulting at the base of the High Himalaya [25,44,45].

The High Himalayan mountain front in NW India forms the main orographic barrier, and at elevations between ~ 2000 and 3500 m more than 80% of the annual precipitation (> 2000 mm/a) of the Indian summer monsoon are forced out [13,46]. This barrier forms a divide between humid areas to the south and more arid sectors (with < 300 mm/a precipitation) to the north. However, where the monsoonal circulation reaches major N–S-oriented valley moisture is also channeled farther into the orogen ([13]; Fig. 1a).

3. Apatite fission track analysis

Apatite Fission Tracks (AFT) are linear damage trails in the crystal lattice that form as the result of spontaneous nuclear fission of trace ^{238}U nuclei [47]. New ^{238}U fission tracks form at an essentially constant rate and with a constant track length, while older tracks simultaneously anneal (and ultimately are erased) at high temperatures, making AFT an effective tool for reconstructing cooling and exhumation histories, e.g. [48–50]. At temperatures hotter than ~ 110 – 150 °C, all fission tracks are totally annealed, resetting the fission track clock to zero. The total annealing temperature (TAT) and the effective closure temperature depend on the kinetic characteristics of the apatite and the cooling rate [51]. The partial annealing zone (PAZ) extends from the TAT down to ~ 60 °C, and within this temperature range tracks are partially annealed. Below ~ 60 °C, AFT are effectively stable because annealing occurs at a very slow rate, e.g. [48]. The kinematic characteristics of apatite can be evaluated by measuring etch pits figures (Dpar, [52]).

All 20 samples for AFT analysis (< 1 – 5 Ma, Fig. 2; details of the sample preparation are listed below Table 2) are bedrock samples collected across the Himalayan Crystalline Core in the Sutlej region. For very young apatites, it may be impossible to obtain

sufficient Dpar data for a robust interpretation. However, several samples with older ages and/or higher U-content yielded multiple measurements for most analyzed crystals, permitting the calculation of closure temperatures [51]. All of the single grain ages in this study pass the chi-squared test, and pooled ages are reported with 2σ errors.

We collected two transects between elevations of 1.5 and 4.5 km to expand the data coverage and add more detail to sites previously sampled for AFT analysis along the Sutlej Valley [6,18]. A ~ 20 km long N–S transect (11 samples) extends along the Wanger Valley and crosses two major tectonic boundaries (MCT and STFS; Fig. 2b). Nearly all samples were collected along the valley bottom. The Sangla transect (five samples; Fig. 2c) was sampled across the hanging wall of the MCT, from the Sutlej river to STFS over an elevation of 2.4 km and horizontal distance of ~ 8 km in the Baspa Valley (Fig. 2).

Samples collected in the High Himalaya near the Sutlej River have <1 – 2 Ma cooling ages, whereas samples at a greater distance from the river yield ages between 3 and 4 Ma (Fig. 2). The lowermost sample of the Wanger Valley transect (1540 m), at the Sutlej riverbank is 0.6 ± 0.4 Ma (RT00-1; $\pm 2\sigma$). The ages increase gradually to 2.8 ± 0.6 Ma at 4460 m (RT00-23; Fig. 2b), the highest sample. Along the Sangla transect samples RT00-42 and -43 (between 1900 and 2000 m) yield ages of 1.2 ± 0.4 and 0.6 ± 0.2 Ma, respectively; at 4400 m, sample RT01-25 yields an age of 3.7 ± 1.2 Ma. Overall, the AFT cooling ages are young. The age trend of both transects is similar within error, with a systematic increase in age with increasing distance to the Sutlej River and rising elevation.

With the exception of one sample, the low spontaneous track density associated with the young AFT ages did not provide track-length data. However, sample RT00-23 has a high U content and an older age; it provided 20 confined tracks ($\bar{\phi} = 14.2 \pm 1.4$ μm). Modelling the age/track-length distribution with the program ‘AFT solve’ [53] confirms continued fast exhumation during Pliocene–Quaternary time, and yields an average cooling rate between ~ 40 and 50 $^{\circ}\text{C}$ for the past 3.5 million years. This is in good agreement with results derived from the age elevation plots (below) and the results of Vannay et al. [6].

The spatial distribution of these new AFT cooling ages are mostly consistent with recently published AFT ages from the Sutlej area [6,18,54], and the Garwhal [55,56] (Fig. 3). AFT ages reported for the Nanga Parbat [57] and Nepal Himalaya, e.g. [8] are even younger. However, because measured AFT ages by Jain et al. [18] in the lower part of LHCS are similar to $^{40}\text{Ar}/^{39}\text{Ar}$ muscovite ages of Vannay et al. [6], they are not considered in our study.

4. Interpretation

AFT ages are interpreted to indicate the elapsed time since cooling below the effective closure temperature. Dpar measurements based on and corrected after Donelick et al. [52] indicate mostly kinetically homogenous samples with a low resistance to annealing. This information suggests an effective closure temperature of 130 ± 10 $^{\circ}\text{C}$ for cooling rates between 10 and 100 $^{\circ}\text{C}/\text{Ma}$ [51]. The young (<5 Ma) AFT cooling ages imply rapid transit through the PAZ, which limits annealing [49]. In addition, these young ages indicate ongoing cooling and exhumation over nearly the entire northwestern SHF (Fig. 3). Interestingly, the AFT ages show no spatial relationship (within error) to structures such as the MCT or STFS (Fig. 2). This is consistent with observations based on AFT and ZFT cooling ages from comparable structural settings as the Kishtwar–Padar–Zanskar region to the northwest (>50 AFT ages, see location #5, 13 and 14 in Fig. 1) [58], where a linear trend in age with increasing elevation is documented.

The mean of 15 AFT cooling ages from the Wanger Valley and Sangla transects is ~ 2 Ma, yielding an average cooling rate of $\sim 65 \pm 5$ $^{\circ}\text{C}/\text{Ma}$ during late Pliocene/Quaternary time. The age-elevation pattern of the Wanger transect shows no discernable deviations from a linear trend, considering the magnitude of uncertainties. We therefore use the simplest possible interpretation of the data: uniform exhumation over the 2.8–0.6 Ma interval at an average rate of $\sim 1.4 \pm 0.2$ mm/a. This is based on the inverse slope of weighted least square regression of the AFT elevation (x) vs. ages $Y(x)$ (Fig. 2). The Sangla transect has cooled within 2.8 Ma (0.9 ± 0.3 Ma [mean of RT00-42 and -43] and 3.7 ± 1.2 Ma), indicating exhumation rates of $\sim 1.1 \pm 0.4$ mm/a.

Minor structural disruptions along transects during these intervals cannot be resolved with the available data, but large disruptions seem improbable. These rates are in good agreement with exhumation rates (1 mm/a for the last 3 Ma) based on modeling results of mineral pairs for the Sutlej region [6]. Comparable exhumation rates from Garwhal [55] (~ 2 mm/a), Central Nepal [8], and the Nanga Parbat [57] (~ 4 mm/a), respectively, are higher. However, because the shallow subsurface temperature distribution is sensitive to the effects of local topography and heat advection by rock-uplift, e.g. [59,60], these exhumation rate estimates must be interpreted with care. Assuming high long-term topographic, erosional, and geothermal steady state for the prolonged exhumation process (active since the Mid Miocene), the perturbations of the isotherms should follow topography with the amplitude, and the perturbation decaying with increasing depth. Therefore, exhumation rates derived from age vs. elevation plots could be overestimated. Modeling results by Safran [61] using a comparable setting to the area described here indicate that our exhumation rates may yield about 60–70% of the true erosion rates. Furthermore, predictions made by Mancktelow and Grasemann (fig. 18 in [60]) suggest that the overestimating are higher than the actual rates. However, it is therefore a possibility that transects are internally deformed in a pervasive manner and that exhumation rates decrease with increasing distance from the Sutlej River. Pervasive brittle normal faulting cutting older structures is ubiquitous and observed across both transects. Alternatively, if the exhumation phase had first started in the Late Miocene–Early Pliocene or accelerated at that time, the apparent exhumation rates could underestimate the true exhumation rates [60]. In fact, modeling results from that uses mineral pairs supports such higher true rates [6].

An impact of hydrothermal activity documented by many hot springs with temperatures 35–70 °C near the bottom of the Sutlej Valley in the LHCS and the HHCS on AFT cooling ages must also be considered [6]. Hydrothermal activity indicates an elevated and steep near-surface geothermal gradient. However, the rather consistently young AFT cooling ages (~ 0.6 –2 Ma) obtained by Jain et al. [18], Vannay et al. [6], and this study indicate smooth local thermal variations and/or that the advective heat flow by hydrothermal

circulation operates in a more pervasive manner. Additional heat advection caused by hydrothermal circulation might induce an additional compression of the isotherms beneath the valley bottom and thereby decrease the amplitude of the perturbed near-surface isotherms.

Our young AFT cooling ages imply that the rocks of the LHCS and the lower parts of the HHCS have experienced rapid exhumation during Late Pliocene/Quaternary time. The potential time lag between the rock uplift associated with heat advection and subsequent cooling implies that uplift detected with the AFT-ages could have commenced somewhat earlier (Late Miocene) or may only display the young phase of continuous exhumation (ongoing since the Mid Miocene). From our data we infer steady (in time) and uniform (in space) exhumation. Before exposing rocks related to the LHCS today, ~ 10 – 15 -km-thick cover units of HHCS had to be removed by localized rapid erosion along the Sutlej Valley. This implies that the exhumation rates can be equated with regional erosion along the Sutlej Valley. Therefore, the young AFT cooling ages and their spatial association with high, and we assume (see below), sustained localized orographic precipitation and fluvial erosion indicate a correlation between climatically driven fluvial erosion and exhumation rates.

5. Discussion

The pattern of AFT cooling ages provides key constraints on Pliocene to Quaternary rock uplift and denudation across the crystalline core of the Sutlej region. All young cooling ages (Fig. 1a and b) are recorded along the southern termination of the Himalayan crystalline core. These areas coincide with focused orographic precipitation, steep longitudinal river profiles [25], high relief and rapid exhumation along a 50–70-km-wide sector, rather than encompassing the entire width of the orogen. This implies a coupling between the distribution of precipitation and exhumation in this region, as summarized in Fig. 4. Topographic and annual precipitation swath profiles (Fig. 4a) perpendicular to the Himalayan range show the strong control of topography over the distribution of orographic precipitation. Thereby the precipitation is focused in sectors with steep topographic gradients

along the Sub-Himalaya and the southern edge of the Lesser Himalayan Thrust Systems (MBT), and between elevations of ~ 2000 and ~ 3500 m along the southern edge of the High Himalaya. The distribution of precipitation is tied to the monsoon pattern [13,46]. About $\sim 80\%$ of the annual precipitation at the SHF falls during the short summer monsoon (June–September), often in intense rainfall events [13,46]. This increased precipitation not only triggers hillslope erosion but also controls the discharge of catchment areas, and is thus an integral part of the fluvial erosion process. According to the stream-power law, river-incision rates should be highest in regions with high runoff and steep river gradients. In addition, the rivers in the Himalayan region are characterized by (1) large annual runoff variation, (2) strong correlation between discharge and sediment transport, and (3) high sediment flux during peak discharge events (e.g., Sutlej River [13]; Ganges River [62]). This implies that the monsoonal precipitation exerts a strong control on erosional surface processes, and due to the high runoff, rivers are able to effectively incise, erode and evacuate sediments to the foreland. This is particularly the case during abnormal monsoon years, which have higher precipitation and longer lasting, intensified monsoon seasons [13]. In order to keep long-term sustained regional erosion in such high mountainous terrains localized, the erosional effluxes have to be balanced by the tectonic influx.

The strongest argument for continuous localized erosion over geologic time scales is the complete removal of the HHCS nappes along the Sutlej Valley, which correlates with approximately 10–15 km of crystalline rock. They once covered the rocks of the LHCS, which are presently exposed in the LKRW (Fig. 2). This sector correlates with the local maximum of average annual precipitation along the Sutlej Valley (Figs. 3 and 4). In addition, exhumation rates of up to 1.5 mm/a ([6] and this study) would be sufficient to remove 10–15 km rocks over a period of 10 Ma. Along the SHF several segments exist, where the HHCS nappes have been completely removed and today rocks related to the LH are exposed in tectonic windows or half windows (Fig. 1a; [27]). This implies that efficient erosion has removed a significant volume of rock since the MCT was active (Fig. 4b). The Indian monsoon has been active with the current synoptic patterns at least since 8 Ma, e.g. [63].

However, continuously high sediment fluxes since Early–Mid Miocene time are reported for the Himalayan foreland basin (SubH), e.g. [64], the Bengal, and Indus fans, e.g. [65–68]. Rocks of the Himalayan crystalline core have dominated the provenance of Himalayan detrital sediments since that time [69]. In addition, due to the continuous unroofing, high-grade metamorphic index minerals have been deposited sequentially in the foreland basin (garnet and staurolite ~ 20 Ma, kyanite ~ 12 Ma, and sillimanite ~ 8 Ma, e.g. [70,71]) with short lag times (~ 1 – 3 Ma) between $^{40}\text{Ar}/^{39}\text{Ar}$ white mica single-grain cooling ages and their depositional ages [72,73]. All these observations indicate rapid exhumation, continuous erosion, and transit of eroded materials to the sedimentary basins. We thus infer that the linked climate and erosion patterns, which we observe today along the SHF, have been sustained during Pliocene–Quaternary time, if not during the entire Late Cenozoic. This environment thus appears to record a strong feedback between monsoonal precipitation, fluvial erosion, and exhumation. Furthermore, increasing climate instability worldwide during the Pliocene–Quaternary may have accelerated the feedback system between erosion, exhumation, and tectonism, e.g. [74,75].

To further assess the extent of high exhumation along the SHF, we compiled available AFT ages (Fig. 3) and available higher temperature thermochronology data. The AFT data show two distinguishable zones of cooling ages. Almost all ages obtained from humid and the monsoon-influenced SHF are young (<1 – 5 Ma) ([6,8,18,54–56,58,76–79], and this paper, see also Figs. 1b and 3). For regions where no published AFT data were available, we used young (2–3 Ma) ZFT cooling ages. Furthermore, $^{40}\text{Ar}/^{39}\text{Ar}$ (4–6 Ma), and Th–Pb monazite data (3–6 Ma) from several transects in Garwhal and Nepal were available (Fig. 1 and Table 1). In contrast to these young ages, AFT cooling ages obtained in arid areas north of the main orographic barrier are 12–15 Ma in southern Tibet [80] (see #11 in Fig. 1 and 6–40 Ma for the internal part of the NW-Himalaya [58,81] (see Fig. 1, #12 and 14). In these areas, like the drier Padar–Zaskar region, exhumation rates are low and only range between 0.1 and 0.3 mm/a for Pliocene–Quaternary time [58,81]. These rocks of the HHCS have thus resided

near the surface since the Mid Miocene. Consequently, due to insufficient precipitation for effective hillslope and fluvial erosion, these sectors of the orogen have been exhumed at much lower rates than comparable rocks along the humid SHF. Due to the lack of adequate thermochronometric data, no long-term exhumation rates of the southern edge of the Lesser and Sub-Himalaya, can be quantified.

Young cooling ages are not only obtained in areas affected by major orogen-traversing rivers like the Tsangpo, Indus, or Sutlej with large catchment areas in the hinterland [6,57,82], but also along longitudinal rivers sourced in the High Himalaya, e.g. [8,55,79]. Despite smaller catchment areas of river networks, these regions apparently collect enough orographic precipitation and therefore have an adequate erosional potential to exhume deeper crustal material. Thus, the distribution of enhanced orographic precipitation plays a more important role in localizing erosion and deformation than the effects of orogen-traversing rivers along the central part of the SHF.

Fig. 4a and c document the correlation between the sector of high topographic gradients, enhanced precipitation and spatial distribution of young cooling ages and exhumation rates. Similar results have also been recently proposed for Central Nepal by Hodges et al. [83]. In the sector of reduced average annual precipitation across the HHCS in the Sutlej Valley the AFT ages are young and still indicate moderate to high exhumation, in good agreement with observation made in Central Nepal. Burbank et al. [8] argued that due to the absence of a trend in the distribution of AFT cooling ages, no direct precipitation–exhumation linkage exists across the SHF, despite a fivefold change in precipitation. However, they neglect to discuss if (1) crustal deformation and the thermal field can be localized in the same way as the partial distribution of precipitation and (2) possible impact of phases of intensified monsoon on different time scales, where increased precipitation penetrated further into the arid sectors of the Himalaya [13]. Recent fluctuations of precipitation and mass flux, similar to those observed during the 2002 monsoon season may represent analogs for more erosive climate conditions in the geologic past [13].

Thus, assessing the relationships between high topography, steep river gradients, orographically controlled erosion and focalized exhumation and defor-

mation over geologic time is crucial for any feedback between erosion and rock-uplift. Several models have been proposed. Hodges et al. [44] suggest that the distribution of gravitational potential energy acts as the driving mechanism to compensate focused erosion by southward extrusion of crustal material. The extrusion of crystalline units like the LHCS today [6] has been inferred to explain the coeval Early–Mid Miocene extrusion of the HHCS between the MCT and STFS [33,36,84]. Coupled thermal mechanical modelling by Beaumont et al. [11] and Jamieson et al. [12] emphasizes the link between ductile extrusion and focused surface denudation. These authors conclude that without erosion, the extrusion of crystalline units would not develop and that rates of exhumation and geometry of the exhuming wedge are sensitive to the erosion parameters.

Alternatively, the Critical Coulomb Wedge theory provides a simple way to explain the interaction between topography, focused erosion, and exhumation. In this context, the erosional loss of material and the geometry of a critical taper are interpreted to be maintained by back-stepping faults such as the MT (Fig. 4a–d) and other back-stepping thrust systems along the SHF [25,44,45,85].

As a third alternative, however, critical taper could also be maintained by underplating. In such a scenario the locality of fast uplift could be due to imbrication of slices from a decollement ramp (Fig. 4b).

Based on our results, we suggest that in order to accommodate the spatially concentrated loss of material along the SHF, focused exhumation and rapid erosion must be coupled with active southward extrusion of high-grade metamorphic units, as has been previously proposed for other parts of the orogen [44,85]. As postulated by Vannay et al. [6], in such a setting extruding high-grade metamorphic rocks along the Sutlej Valley would be bounded to the south by the MT at their base and by the KNFZ at their top, (Fig. 4b). In Garwhal and Kumaun, to the SE (#2 and 3 in Fig. 1) the MT is recognized over a long distance along strike [40,86] where monsoonal precipitation affects the High Himalaya over a broad sector (Fig. 1a). Toward the NW the MT only appears in a tectonic window across Sutlej Valley (Fig. 4) and diminishes in throw. The decrease in throw is mimicked by a decrease in monsoonal precipitation from east to west. Thus, a back-stepping thrust appears to have devel-

oped only in those regions affected by high rainfall, strong erosion and exhumation, which indicates a close correlation between removal of large volume of rock and the magnitude of fault offset to balance loss of material.

In summary, these observations imply that localized erosion as described here is a first-order process during shortening, when a mountain belt is favorably oriented in order to intercept moisture-bearing winds. This in turn determines renewed faulting in the internal part of the Himalayan orogen, and thus a more diachronous pattern of deformation pattern of deformation in the mountain belt.

6. Conclusions

The Himalaya is probably a unique location to improve our understanding of the couplings between surface and tectonic processes. The AFT data obtained from the Himalayan Crystalline Core along two elevation transects crossing major tectonic structures are between <1 and 4 Ma. Assuming a simplified denudation with long-term steady-state erosion and exhumation, the rocks were exhumed with $\sim 1.4 \pm 0.2$ and 1.1 ± 0.4 mm/a with an average cooling of ~ 40 – 50 °C/Ma during Pliocene–Quaternary time. An important finding is that the sample transects correlate with distance, but show no spatial relationship (within error) to structures such as the MCT or STFS. The distribution of AFT cooling ages across the Sutlej region and the correlation between areas of focused orographic precipitation and high topography imply a strong interaction between rapid erosion, exhumation, and sediment evacuation that is concentrated in a ~ 50 – 70 -km-wide sector of the Himalayan deformation belt (Fig. 4a–d). To compensate this redistribution of material, back-stepping thrusts are activated which displace the crystalline core of the high Himalaya as an extruding wedge bounded by passive normal faults at the top, also recently suggested by Vannay et al. [6] and Wobus et al. [45]. The denudational loss of material is balanced by tectonic uplift through a coupling between surface processes and internal deformation of the orogen at depth. Thus, surface processes control the internal deformation along the SHF.

Acknowledgements

The authors would like to thank: A.K. Jain and S. Singh for valuable discussions and logistical support; B. Grasemann, C. Janda, C. Hager, E. Draganits, and J.-C. Vannay for introducing us to the spectacular geology of the Himalaya and granting access to unpublished data; the great Indian mountain guides S. Slathia and T. Tsering for support during fieldwork; and E. Stump, G. Hilley and S. Peacock for discussion and comments on an earlier version of this manuscript. We very much appreciate the reviews by M. Brandon and K. Hodges with detailed comments and suggestions that improved the manuscript significantly. We thank the Deutsche Forschungsgemeinschaft (DFG) for financial support (Grant #STR-11/4), and the DAAD for support of R.T. while at Arizona State University (ASU). [KF]

References

- [1] P.O. Koons, The two-sided orogen: collision and erosion from the sand box to the Southern Alps, *Geology* 18 (1990) 679–682.
- [2] K.X. Whipple, G.E. Tucker, Dynamics of the stream power river incision model: implications for height limits of mountain ranges, landscape response time scales and research needs, *Journal of Geophysical Research* 104 (1999) 17661–17674.
- [3] S.D. Willett, Orogeny and orography: the effects of erosion on the structure of mountain belts, *Journal of Geophysical Research* 104 (1999) 28957–28982.
- [4] R.E. Horton, Erosional development of streams and their drainage basins, hydrophysical approach to quantitative morphology, *Geological Society of America Bulletin* 56 (3) (1945) 275–370.
- [5] P.K. Zeitler, A.S. Meltzer, P.O. Koons, D. Craw, B. Hallet, C.P. Chamberlain, W.S.F. Kidd, S.K. Park, L. Seeber, M. Bishop, J. Shroder, Erosion, Himalayan geodynamics, and the geomorphology of metamorphism, *GSA Today* 11 (2001) 4–9.
- [6] J.C. Vannay, B. Grasemann, M. Rahn, W. Frank, A. Carter, V. Baudraz Cosca M., Miocene to Holocene exhumation of metamorphic crustal wedges in the Himalayan orogen: evidence for tectonic extrusion coupled to fluvial erosion, *Tectonics* 23 (2004) (TC1014).
- [7] D. Davis, J. Suppe, F.A. Dahlen, Mechanics of fold-and-thrust belts and accretionary wedges, *Journal of Geophysical Research* 88 (1983) 1153–1172.
- [8] D.W. Burbank, A.E. Blythe, J. Putkonen, B. Pratt-Sitaula, E. Gabet, M. Oskin, A. Barros, T.P. Ojha, Decoupling of erosion and precipitation in the Himalayas, *Nature* 426 (6967) (2003) 652–655.
- [9] P.W. Reiners, T.A. Ehlers, S.G. Mitchell, D.R. Montgomery,

- Coupled spatial variations in precipitation and long-term erosion rates across the Washington Cascades, *Nature* 426 (6967) (2003) 645–647.
- [10] S.J. Dadson, N. Hovius, H.G. Chen, W.B. Dade, M.L. Hsieh, S.D. Willett, J.C. Hu, M.J. Hornig, M.C. Chen, C.P. Stark, D. Lague, J.C. Lin, Links between erosion, runoff variability and seismicity in the Taiwan orogen, *Nature* 426 (6967) (2003) 648–651.
- [11] C. Beaumont, R.A. Jamieson, M.H. Nguyen, B. Lee, Himalayan tectonics explained by extrusion of a low-viscosity crustal channel coupled to focused surface denudation, *Nature* 414 (2001) 738–742.
- [12] R.A. Jamieson, C. Beaumont, M.H. Nguyen, B. Lee, Interaction of metamorphism, deformation and exhumation in large convergent orogens, *Journal of Metamorphic Geology* 20 (1) (2002) 9–24.
- [13] B. Bookhagen, R. Thiede, M.R. Strecker. Extreme Monsoon events and their control on erosion and sediment flux in the high, arid NW Himalayas, *Earth and Planetary Science Letters*, in review.
- [14] P. Copeland, T.M. Harrison, K.V. Hodges, P. Maruejol, P. Le Fort, A. Pecher, An early Pliocene thermal disturbance of the Main Central Thrust, central Nepal: implications for Himalayan tectonics, *Journal of Geophysical Research* 96 (B5) (1991) 8475–8500.
- [15] R.P. Metcalfe, Pressure, temperature and time constraints on metamorphism across the Main Central Thrust zone and high Himalayan slab in the Garhwal Himalaya, in: P.J. Treloar, M.P. Searle (Eds.), *Himalayan Tectonics*, Geological Society Special Publications 74 (1993) 485–509.
- [16] T.M. Harrison, F.J. Ryerson, P. Le Fort, A. Yin, O.M. Lovera, E.J. Catlos, A late Miocene–Pliocene origin for the central Himalayan inverted metamorphism, *Earth and Planetary Science Letters* 146 (1–2) (1997) E1–E7.
- [17] T.M. Harrison, M. Grove, O.M. Lovera, E.J. Catlos, J. D’Andrea, The origin of Himalayan anatexis and inverted metamorphism: models and constraints, *Journal of Asian Earth Sciences* 17 (5–6) (1999) 755–772.
- [18] A.K. Jain, D. Kumar, S. Singh, A. Kumar, N. Lal, Timing, quantification and tectonic modelling of Pliocene–Quaternary movements in the NW Himalaya: evidence from fission track dating, *Earth and Planetary Science Letters* 179 (3–4) (2000) 437–451.
- [19] E.J. Catlos, T.M. Harrison, M.J. Kohn, M. Grove, F.J. Ryerson, C.E. Manning, B.N. Upreti, Geochronologic and thermobarometric constraints on the evolution of the Main Central Thrust, central Nepal Himalaya, *Journal of Geophysical Research-Solid Earth* 106 (B8) (2001) 16177–16204.
- [20] E.J. Catlos, T.M. Harrison, C.E. Manning, M. Grove, S.M. Rai, M.S. Hubbard, B.N. Upreti, Records of the evolution of the Himalayan orogen from in situ Th–Pb ion microprobe dating of monazite: eastern Nepal and western Garhwal, *Journal of Asian Earth Sciences* 20 (5) (2002) 459–479.
- [21] C.T. Klootwijk, J.S. Gee, J.W. Pierce, G.M. Smith, P.L. McFadden, An early India–Asia contact: paleomagnetic constraints from Ninetyeast Ridge, ODP Leg 121, *Geology* 20 (1992) 395–398.
- [22] K.V. Hodges, Tectonics of the Himalaya and southern Tibet from two perspectives, *Geological Society of America Bulletin* 112 (2000) 324–350.
- [23] R. Bilham, K. Larson, J. Freymuller, J. P.I. members, GPS measurements of present-day convergence across the Nepal Himalaya, *Nature* 386 (1997) 61–64.
- [24] M.R. Pandey, R.P. Tandukar, J.P. Avouac, J. Lave, J.P. Massot, Interseismic strain accumulation on the Himalayan crustal ramp (Nepal), *Geophysical Research Letters* 22 (7) (1995) 751–754.
- [25] L. Seeber, V. Gornitz, River profiles along the Himalayan arc as indicators of active tectonics, *Tectonophysics* 92 (1983) 335–367.
- [26] C. Duncan, J. Masek, E. Fielding, How steep are the Himalaya? Characteristics and implications of along-strike topographic variations, *Geology* 31 (1) (2003) 75–78.
- [27] A. Gansser, *Geology of the Himalayas*, Interscience, London, 1964, 289 pp.
- [28] W. Zhao, K.D. Nelson, P.I. Team, Deep seismic reflection evidence of continental underthrusting beneath southern Tibet, *Nature* 366 (1993) 557–559.
- [29] P. Lefort, Himalayas-collided range-present knowledge of continental arc, *American Journal of Science* A275 (1975) 1.
- [30] J.C. Vannay, B. Grasemann, Inverted metamorphism in the High Himalaya of Himachal Pradesh (NW India): phase equilibria versus thermobarometry, *Schweizerische Mineralogische und Petrographische Mitteilungen* 78 (1) (1998) 107–132.
- [31] M.E. Coleman, U–Pb constraints on Oligocene–Miocene deformation and anatexis within the central Himalaya, Marsyandi Valley, Nepal, *American Journal of Science* 298 (7) (1998) 553–571.
- [32] M.S. Hubbard, T.M. Harrison, Ar-40/Ar-39 Age constraints on deformation and metamorphism in the main central thrust zone and Tibetan slab, Eastern Nepal Himalaya, *Tectonics* 8 (4) (1989) 865–880.
- [33] B.D. Burchfiel, C. Zhileng, K.V. Hodges, L. Yuping, L.H. Royden, D. Changrong, X. Jiene, The South Tibetan detachment system, Himalayan orogen: extension contemporaneous with and parallel to shortening in a collisional mountain belt, *Special Paper-Geological Society of America* 269 (1992) 1–41.
- [34] J.P. Burg, M. Brunel, D. Gapais, G.M. Chen, G.H. Liu, Deformation of leucogranites of the crystalline main central sheet in Southern Tibet (China), *Journal of Structural Geology* 6 (5) (1984) 535.
- [35] P.J. Dezes, J.C. Vannay, A. Steck, F. Bussy, M. Cosca, Synorogenic extension: quantitative constraints on the age and displacement of the Zaskar shear zone (northwest Himalaya), *Geological Society of America Bulletin* 111 (3) (1999) 364–374.
- [36] B. Grasemann, H. Fritz, J.C. Vannay, Quantitative kinematic flow analysis from the Main Central Thrust Zone (NW-Himalaya, India): implications for a decelerating strain path and the extrusion of orogenic wedges, *Journal of Structural Geology* 21 (7) (1999) 837–853.
- [37] J. Vannay, B. Grasemann, Himalayan inverted metamorphism

- and syn-convergence extension as a consequence of a general shear extrusion, *Geological Magazine* 3 (2001) 253–276.
- [38] A. Pecher, The metamorphism in the Central Himalaya, *Journal of Metamorphic Geology* 7 (1) (1989) 31–41.
- [39] W. Frank, B. Grasemann, P. Guntli, C. Miller, Geological map of the Kishtwar–Chamba–Kulu region (NW Himalayas, India), *Jahrbuch der Geologischen Bundesanstalt* 138 (1995) 208–299.
- [40] K.S. Valdiya, *Geology of the Kumaun Lesser Himalaya*, Wadia Institute of Himalayan Geology, Dehra Dun, 1980, 291 pp.
- [41] C. Hager, C. Janda, B. Grasemann, E. Draganits, J.C. Vannay, Active extrusion in the Sutlej Valley (NW-Himalaya), *Geophysical Research Abstracts*, vol. 5 (06944), European Geophysical Society, Nice, 2003.
- [42] D. Schelling, K. Arita, Thrust tectonics, crustal shorting, and the structure of the far-eastern Nepal Himalaya, *Tectonics* 10 (5) (1991) 851–862.
- [43] R. Cattin, J.P. Avouac, Modeling mountain building and the seismic cycle in the Himalaya of Nepal, *Journal of Geophysical Research-Solid Earth* 105 (B6) (2000) 13389–13407.
- [44] K.V. Hodges, J.M. Hurtado, K.X. Whipple, Southward extrusion of Tibetan crust and its effect on Himalayan tectonics, *Tectonics* 20 (2001) 799–809.
- [45] C.W. Wobus, K.V. Hodges, K.X. Whipple, Has focused denudation sustained active thrusting at the Himalayan topographic front? *Geology* 31 (10) (2003) 861–864.
- [46] A.P. Barros, M. Joshi, J. Putkonen, D.W. Burbank, A study of the 1999 monsoon rainfall in a mountainous region in central Nepal using TRMM products and rain gauge observations, *Geophysical Research Letters* 27 (2000) 3683–3686.
- [47] G. Wagner, P. Van den Haute, *Fission Track Dating*, Kluwer Academic Publishing, Dordrecht, Netherlands, 1992, 285 pp.
- [48] A.J.W. Gleadow, I.R. Duddy, P.F. Green, J.F. Lovering, Confined fission track lengths in apatite: a diagnostic tool for thermal history analysis, *Contributions to Mineralogy and Petrology* 94 (1986) 405–415.
- [49] P.F. Green, I.R. Duddy, G.M. Laslett, K.A. Hegarty, A.J.W. Gleadow, J.F. Lovering, Thermal annealing of fission tracks in apatite: 4. Quantitative modelling techniques and extension to geological timescales, *Chemical Geology. Isotope Geoscience Section* 79 (1989) 155–182.
- [50] T.A. Dumitru, Fission-track geochronology, in: J.S. Noller, J.M. Sowers, W.R. Lettis (Eds.), *Quaternary Geochronology; Methods and Applications*, American Geophysical Union, Washington, DC, 2000, pp. 131–155.
- [51] R.A. Ketcham, R.A. Donelick, W.D. Carlson, Variability of apatite fission-track annealing kinetics: III. Extrapolation to geologic time scales, *American Mineralogist* 84 (1999) 1235–1255.
- [52] R.A. Donelick, R.A. Ketcham, W.D. Carlson, Variability of apatite fission-track annealing kinetics: II. Crystallographic orientation effects, *American Mineralogist* 84 (9) (1999) 1224–1234.
- [53] R.A. Ketcham, R.A. Donelick, M.B. Donelick, AFTSolve: a program for multikinetic modeling of apatite fission-track data, *American Mineralogist* 88 (5–6) (2003) 929.
- [54] N. Lal, Y.D. Mehta, D. Kumar, A. Kumar, A.K. Jain, Cooling and exhumation history of the Mandi granite and adjoining tectonic units, Himachal Pradesh, and estimation of closure temperature from external surface of zircon, in: A.K. Jain, R.M. Manickavasagam (Eds.), *Geodynamic of the NW Himalaya*, Gondwana Res. Group Mem., 6 (1999) 207–216.
- [55] R.B. Sorkhabi, E. Stump, K.A. Fol, A.K. Jain, Fission-track and Ar-40/Ar-39 evidence for episodic denudation of the Gangotri granites in the Garhwal Higher Himalaya, India, *Tectonophysics* 260 (1–3) (1996) 187–199.
- [56] M.P. Searle, S.R. Noble, A.J. Hurford, D.C. Rex, Age of crustal melting, emplacement and exhumation history of the Shivling leucogranite, Garhwal Himalaya, *Geological Magazine* 136 (5) (1999) 513–525.
- [57] P.K. Zeitler, Cooling history of the NW Himalaya, Pakistan, *Tectonics* 4 (1985) 127–151.
- [58] A. Kumar, N. Lal, A.K. Jain, R.B. Sorkhabi, Late cenozoic–quaternary thermo-tectonic history of higher Himalayan Crystalline (Hhc) in Kishtwar–Padar–Zaskar Region, Nw Himalaya—Evidence from fission-track ages, *Journal of the Geological Society of India* 45 (4) (1995) 375–391.
- [59] K. Stuwe, L. White, R. Brown, The influence of eroding topography on steady-state isotherms—application to fission-track analysis, *Earth and Planetary Science Letters* 124 (1–4) (1994) 63–74.
- [60] N.S. Mancktelow, B. Grasemann, Time-dependent effects of heat advection and topography on cooling histories during erosion, *Tectonophysics* 270 (1997) 167–195.
- [61] E.B. Safran, Geomorphic interpretation of low-temperature thermochronologic data: insights from two-dimensional thermal modeling, *Journal of Geophysical Research-Solid Earth* 108 (B4) (2003) (2189).
- [62] A. Galy, C. France-Lanord, Higher erosion rates in the Himalaya: geochemical constraints on riverine fluxes, *Geology* 29 (2001) 23–26.
- [63] W.L. Prell, J.E. Kutzbach, Sensitivity of the Indian monsoon to forcing parameters and implications for its evolution, *Nature* 360 (6405) (1992) 647–652.
- [64] D.W. Burbank, R.A. Beck, T. Mulder, The Himalayan Foreland, in: Y. An, T.M. Harrison (Eds.), *Asian Tectonics*, Cambridge Univ. Press, Cambridge, 1996, pp. 149–188.
- [65] P. Copel, M.T. Harrison, Episodic rapid uplift in the Himalaya revealed by $^{40}\text{Ar}/^{39}\text{Ar}$ analysis of detrital K-felspar and muscovite, Bengal fan, *Geology* 18 (1990) 354–359.
- [66] F. Métivier, Y. Guademer, P. Tapponier, M. Klein, Mass accumulation rates in Asia during the Cenozoic, *Geophysical Journal International* 137 (1999) 280–318.
- [67] G. Einsele, L. Ratschbacher, A. Wetzel, The Himalaya–Bengal fan denudation–accumulation system during the past 20 Ma, *Journal of Geology* 104 (1996) 163–184.
- [68] P. Clift, C. Gaedicke, Accelerated mass flux to the Arabian Sea during the middle to late Miocene, *Geology* 30 (3) (2002) 207–210.
- [69] L.A. Derry, C. France-Lanord, Himalayan weathering and erosion fluxes: climate and tectonic controls, in: W.F. Ruddiman (Ed.), *Tectonic Uplift and Climate Change*, Plenum, New York, 1997, pp. 290–312.
- [70] Y. Najman, M. Pringle, M. Bickle, E. Garzanti, D. Burbank, S.

- Ando, N. Brozovic', Non-steady-state exhumation of the Higher Himalaya, N.W. India: insights from a combined isotopic and sedimentological approach, Geophysical Research Abstracts vol. 5, European Geophysical Society, Nice, 2003.
- [71] Y. Najman, E. Garzanti, M. Pringle, M. Bickle, S. Ando, N. Brozovic, Exhumation and attainment of steady state in the Himalaya: insights from the detrital sediment record, EOS (Transactions-American Geophysical Union) 83 (2002) F1302.
- [72] T.M. Harrison, P. Copeland, S.A. Hall, J. Quade, S. Burner, T.P. Ojha, W.S.F. Kidd, Isotopic preservation of Himalayan/Tibetan uplift, denudation, and climatic histories in the molasse deposits, Journal of Geology 101 (1993) 157–175.
- [73] N.M. White, M. Pringle, E. Garzanti, M. Bickle, Y. Najman, H. Chapman, P. Friend, Constraints on the exhumation and erosion of the High Himalayan Slab, NW India, from foreland basin deposits, Earth and Planetary Science Letters 195 (2002) 29–44.
- [74] P. Molnar, P. England, Late Cenozoic uplift of mountain ranges and global climatic change: chicken or egg? Nature 346 (1990) 29–34.
- [75] P. Zhang, P. Molnar, W.R. Downs, Increased sedimentation rates and grain sizes 2–4 Myr ago due to the influence of climate change on erosion rates, Nature 410 (2001) 891–897.
- [76] R.B. Sorkhabi, Time–temperature pathways of Himalayan and Trans-Himalayan crystalline rock: a comparison of fission-track ages, Nuclear Tracks and Radiation Measurements 21 (1993) 535–542.
- [77] R.B. Sorkhabi, E. Stump, K.A. Foland, Late Pliocene denudation chronology of the main central thrust Hangingwall in Solu Himal, Nepal, EOS Trans. American Geophysical Union 81 (48) (2003) (Fall Meet. Suppl. T51C-05).
- [78] P. Copeland, P. Le Fort, P. Henry, S.M. Rai, D.A. Foster, R.R. Pecher, A. Pecher, K. Stuwe, B.N. Upreti, Twenty million years of thrusting near Kathmandu: everything in order here, EOS Trans. American Geophysical Union 80 (1999) (Fall Meet. Suppl. T31E-04).
- [79] A.V. Bojar, H. Fritz, M. Bregar, S. Nicolescu, P. Reiners, F. Neubauer, R. Handler, Quaternary exhumation and cooling of the central Himalayas by reactivation of Miocene faults: evidence from structures, $^{40}\text{Ar}/^{39}\text{Ar}$, fission-track, and U-Th/He data, Geophysical Research Abstracts, vol. 5 (08623), European Geophysical Society, Nice, 2003.
- [80] M.P. Searle, R.R. Parrish, K.V. Hodges, A. Hurford, M.W. Ayres, M.J. Whitehouse, Shisha Pangma leucogranite, south Tibetan Himalaya: field relations, geochemistry, age, origin, and emplacement, Journal of Geology 105 (3) (1997) 295–317.
- [81] M. Schlup, A. Carter, M. Cosca, A. Steck, Exhumation history of eastern Ladakh revealed by Ar-40/Ar-39 and fission-track ages: the Indus River-Tso Morari transect, NW Himalaya, Journal of the Geological Society 160 (2003) 385–399.
- [82] J.-P. Burg, P. Davy, P. Nievergelt, F. Oberli, D. Seward, Z. Diao, M. Meier, Exhumation during crustal folding in the Namche–Barwa syntaxis, Terra Nova 9 (1997) 53–56.
- [83] K.V. Hodges, C.W. Wobus, K. Ruhl, S. Taylor, K.X. Whipple, Quaternary deformation, river steepening, and heavy precipitation at the front of the Higher Himalayan ranges, Earth and Planetary Science Letters doi:10.1016/j.epsl.2004.01.019.
- [84] K.V. Hodges, R.R. Parrish, T.B. Housh, D.R. Lux, B.C. Burchfiel, L.H. Royden, Z. Chen, Simultaneous miocene extension and shortening in the Himalayan Orogen, Science 258 (5087) (1992) 1466–1470.
- [85] D. Grujic, L.S. Hollister, R.R. Parrish, Himalayan metamorphic sequence as an orogenic channel: insight from Bhutan, Earth and Planetary Science Letters 198 (1–2) (2002) 177–191.
- [86] K.S. Valdiya, The 2 intracrustal boundary thrusts of the Himalaya, Tectonophysics 66 (4) (1980) 323–348.
- [87] P.F. Green, A new look at statistics in fission-track dating, Nuclear Tracks and Radiation Measurements 5 (1981) 77–86.
- [88] R.F. Galbraith, On statistical-models for fission-track counts, Journal of the International Association for Mathematical Geology 13 (6) (1981) 471–478.
- [89] R.F. Galbraith, G.M. Laslett, Statistical models for mixed fission-track ages, Nuclear Tracks and Radiation Measurements 21 (1993) 459–470.
- [90] A.J. Hurford, P.F. Green, The zeta-age calibration of fission-track dating, Isotope Geoscience 1 (4) (1983) 285–317.
- [91] T.A. Dumitru, A new computer-automated microscope stage system for fission-track analysis, Nuclear Tracks and Radiation Measurements 21 (4) (1993) 575–580.
- [92] I. Dunkl, Trackkey: a windows program for calculation and graphical presentation of fission track data, Computers & Geosciences 28 (1) (2002) 3–12.
- [93] J.C. Vannay, Z.D. Sharp, B. Grasemann, Himalayan inverted metamorphism constrained by oxygen isotope thermometry, Contributions to Mineralogy and Petrology 137 (12) (1999) 90–101.
- [94] R.M. Edwards, $^{40}\text{Ar}/^{39}\text{Ar}$ geochronology of the Main Central thrust (MCT) region: evidence for Late Miocene to Pliocene disturbances along the MCT, Marsyangdi River valley, west-central Nepal Himalaya, Journal of Nepal Geological Society 10 (1995) 41–46.
- [95] P. Gautam, S. Koshimizu, Zircon and apatite fission track dating of the Ampipal alkaline massif, the Nepal Lesser Himalaya, Journal of Nepal Geological Society 7 (1991) 1–8.
- [96] K. Arita, Thrust tectonics and uplift process of the Nepal Himalaya revealed from fission-track ages, Chigaku Zasshi (Journal of Geography) 1062 (951) (1997) 156–167.